Green Chemistry

PAPER

View Article Online
View Journal | View Issue

Cite this: *Green Chem.*, 2021, **23**, 3073

Ruthenium complex immobilized on supported ionic-liquid-phase (SILP) for alkoxycarbonylation of olefins with CO_2†

Shi-Ping Xia,[a,b] Guang-Rong Ding,[b,c] Rui Zhang, *[a] Li-Jun Han,[b] Bao-Hua Xu *[b,c] and Suo-Jiang Zhang [b,c]

In this study, the heterogeneously catalyzed alkoxycarbonylation of olefins with CO_2 based on a supported ionic-liquid-phase (SILP) strategy is reported for the first time. An [Ru]@SILP catalyst was accessed by immobilization of ruthenium complex on a SILP, wherein imidazolium chloride was chemically integrated at the surface or in the channels of the silica gel support. An active Ru site was generated through reacting $Ru_3(CO)_{12}$ with the decorated imidazolium chloride in a proper microenvironment. Different IL films, by varying the functionality of the side chain at the imidazolium cation, were found to strongly affect the porosity, active Ru sites, and CO_2 adsorption capacity of [Ru]@SILP, thereby considerably influencing its catalytic performance. The optimized [Ru]@SILP-A-2 displayed enhanced catalytic performance and prominent substrate selectivity compared to an independent homogeneous system under identical conditions. These findings provide the basis for a novel design concept for achieving both efficient and stable catalysts in the coupling of CO_2 with olefins.

Received 28th December 2020,
Accepted 25th March 2021

DOI: 10.1039/d0gc04386a

rsc.li/greenchem

Introduction

Converting CO_2 into high value-added chemicals and fuels is regarded as one of the most promising technologies by which to alleviate the energy and environmental crisis.[1–6] To date, a variety of strategies on using CO_2 as a C1 surrogate in the alkoxycarbonylation of olefins have been documented.[7–10] Therein, the reductive conversion of CO_2 to CO with proper reductants[11–13] imitating the reverse water gas shift process, followed by the alkoxycarbonylation of olefins, has attracted the most attention. In this regard, researchers have focused on the construction of novel homogeneous systems consisting of non-noble metals and phosphine-free ligands over the past decade to meet the global goal of sustainable development.[14] However, heterogeneous catalysts are preferred industrially due to their low cost and ease of separation and reuse. Therefore, supported transition-metal nanoparticles have been used to promote the conversion of CO_2 to fine chemicals.[15–19] To achieve the alkoxycarbonylation of olefins using CO_2, supported ionic-liquid-phase (SILP)[20–22] heterogeneous catalysts have the potential for use as sustainable heterogeneous catalysts with a homogeneous microenvironment around the active site, but to date these have remained unexplored.

SILP candidates can be accessed by the confinement or covalent tethering of a well-stabilized thin layer of ionic liquid (IL) in a highly porous matrix. In principle, the properties, including the structural patterns and functionality at or near interfaces, porosity, and interaction force between the IL film and the carrier, can be readily modified by judiciously coupling selected ILs and porous materials. Upon incorporation with various transition-metal complexes[23–26] or nanoparticles,[27–30] SILPs have been employed in flow processes for gas phase reactions such as hydroformylation,[31–34] hydrogenation,[35–38] the water–gas shift reaction,[39–41] the reverse water–gas shift reaction[42] and hydroaminomethylation.[43] Experimental investigations into the approach of the SILP-mediated alkoxycarbonylation of olefins with CO_2 and studies on the reactivity difference between selected IL films with the same carriers would lead to a better understanding of how the parameters of SILPs influence the catalyst and further advance the potential of such strategies.

Based on the present understanding on the homogeneous $Ru_3(CO)_{12}$-catalyzed alkoxycarbonylation of olefins with CO_2 in imidazolium chlorides, either abnormal $C^{4/5}$ or normal C^2

[a]State Key Laboratory of Chemical Engineering, East China University of Science and Technology, Shanghai 200237, China. E-mail: r.zhang@ecust.edu.cn
[b]Beijing Key Laboratory of Ionic Liquids Clean Processes, CAS Key Laboratory of Green Processes and Engineering, State Key Laboratory of Multiphase Complex Systems, Institute of Process Engineering, Chinese Academy of Sciences, 100190 Beijing, China. E-mail: bhxu@ipe.ac.cn
[c]School of Chemistry and Chemical Engineering, University of Chinese Academy of Sciences, Beijing 100049, China

†Electronic supplementary information (ESI) available. See DOI: 10.1039/d0gc04386a

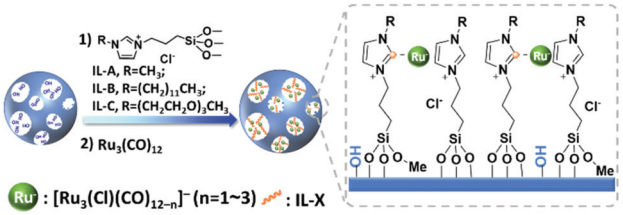

Scheme 1 Schematic illustration of the preparation of [Ru]@SILP hybrids.

mode NHC carbene ligated Ru species have been detected *in situ* as the active site.[44–48] Besides this, the presence of Cl^- facilitates the deprotonation of the transient ruthenium hydride species to enable the activation of CO_2 by coordination. It is also supposedly crucial for the formation of $[Ru_3(Cl)(CO)_{12-n}]^-$ (n = 1–3) species, where the strong anti-effect of Cl^- therein accelerates CO dissociation and olefin association for alkoxycarbonylation.[49–53] We thus envisioned the design and fabrication of novel [Ru]@SILP hybrids in an adaptable and controlled manner, wherein task-specific imidazolium chloride are covalently decorated in the porous support, followed by the immobilization of Ru *via* direct reaction with $Ru_3(CO)_{12}$ (Scheme 1). The quantity of Ru active sites can be controlled through the ratio of $Ru_3(CO)_{12}$ to imidazolium units located within a proper microenvironment. As a proof of concept, commercially available porous silica gel was examined as a carrier. The difference between representative functionalities (Me (X = A), $C_{12}H_{25}$ (X = B), $(CH_2CH_2O)_3CH_3$ (X = C)) at the side chain of the imidazolium ring on the physicochemical properties of the SILP and thereby the catalytic performance of [Ru]@SILP was investigated. Impressively, [Ru]@SILP-A-2 exhibits durable catalytic activity, recyclability, and applicability in the alkoxycarbonylation of olefins with CO_2, which was performed in the presence of methanol (MeOH) and provides methoxyl carbonylate products in good yields. Moreover, [Ru]@SILP-A-2 exhibits enhanced catalytic performance compared to an individual homogeneous catalyst, attributed to its highly dispersed catalytic sites, porous framework with high surface area, and large CO_2 adsorption capacity and enrichment. Besides this, it shows prominent substrate selectivity, wherein small cyclic olefins and short-chain linear olefins are preferred, corresponding to the steric hindrance effect of the pore channels. These findings provide a platform for novel design concept to achieve both efficient and stable SILP catalysis in the coupling of CO_2 with olefins.

Results and discussion

Synthesis and characterization of [Ru]@SILP hybrids

The synthesis of [Ru]@SILP hybrids, denoted as [Ru]@SILP-X-m, was conducted through the chemical functionalization of silica gel with IL-X to form SILP[Cl]-X, followed by reaction with a certain amount of $Ru_3(CO)_{12}$. In the label, X represents the type of IL incorporated (1-R-3-(trimethoxysilyl)propyl imidazolium chloride (R = Me (X = A), $C_{12}H_{25}$ (X = B), $(CH_2CH_2O)_3CH_3$ (X = C)) and m indicates the amount of $Ru_3(CO)_{12}$ added (m = 1, $Ru_3(CO)_{12}$ = 19 mg; m = 2, $Ru_3(CO)_{12}$ = 38 mg; m = 3, $Ru_3(CO)_{12}$ = 76 mg).

The porosity of [Ru]@SILP-X-2 (X = A, B, C) and the silica gel support was investigated through carrying out nitrogen-sorption isotherms at 77 K (Fig. 1). All of the samples displayed a typical type IV isotherm featuring a rapid uptake at a low relative pressure at $P/P_0 < 0.01$, followed by a sharp step at $0.40 < P/P_0 < 0.80$, which is characteristic of a mesoporous skeleton (Fig. 1a). The Brunauer–Emmett–Teller (BET) surface area of [Ru]@SILP-X-2 was determined to be 324 $m^2\ g^{-1}$ (X = A), 384 $m^2\ g^{-1}$ (X = B), 113 $m^2\ g^{-1}$ (X = C), respectively, suggesting pore accessibility therein, although the values were all lower compared to those of the silica gel support (514 $m^2\ g^{-1}$, Table S1†). Besides this, the average pore size of [Ru]@SILP-X-2 is almost the same (3.6 nm) with different IL moieties (Fig. 1b), but the volume decreases in the order of A (0.443 $cm^3\ g^{-1}$) > B (0.404 $cm^3\ g^{-1}$) > C (0.128 $cm^3\ g^{-1}$) (Table S1†). We also found that both the BET surface area and Barrett–Joyner–Halenda (BJH) pore size distribution of [Ru]@SILP-A-m deceases slightly with increasing Ru content (Fig. S1†), wherein the maximum Ru per mass unit of SILP[Cl]-A was controlled at less than 2.5 wt% (Table S2†). These results suggest that both the surface and channel of the silica gel is partially occupied by the ILs and Ru.

The morphologies of [Ru]@SILP-X-2 and the silica gel support were characterized *via* a combination of scanning electron microscopy (SEM) and transmission electron microscopy (TEM) (Fig. 2). Apparently, the silica gel exhibits an amorphous and porous structure consisting of some aggregates of small particles (Fig. 2a). In comparison, the surface of [Ru]@SILP-X-2 is much rougher since the size and quantity of the aggregates increased, suggesting the IL is partially immobilized on the silica gel. However, no significant difference in morphology was detected between [Ru]@SILP-A-2, [Ru]@SILP-B-2 and [Ru]@SILP-C-2. The EDS elemental mapping clearly reveals that Ru is uniformly located on the surface of the hybrids (Fig. 2b), thus indicating that both the IL moieties and Ru species are highly dispersed on the silica gel support. In addition, the density of Ru in [Ru]@SILP-B-2 bin the EDS

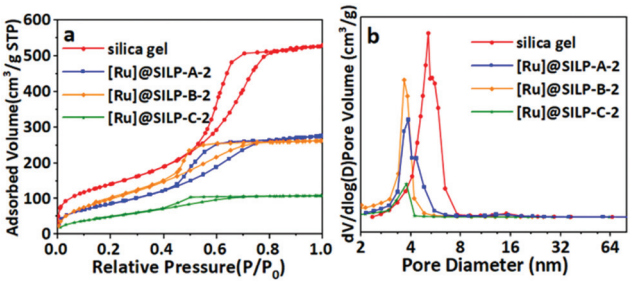

Fig. 1 (a) N_2 adsorption isotherms and (b) BJH pore size distribution of silica gel; [Ru]@SILP-A-2; [Ru]@SILP-B-2 and [Ru]@SILP-C-2.

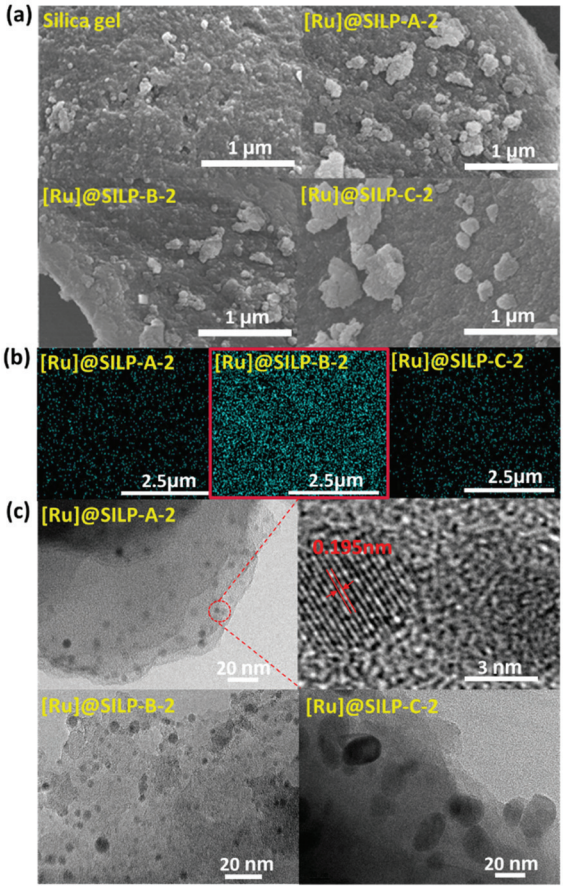

Fig. 2 The morphology and microstructure of [Ru]@SILP-X-2 (a) SEM images of silica gel and [Ru]@SILP-X-2 (X = A, B and C); (b) EDS analysis of Ru in [Ru]@SILP-X-2 (X = A, B and C); (c) HR-TEM images of [Ru]@SILP-X-2 (X = A, B and C).

elemental mapping is apparently higher than that in [Ru]@SILP-A-2 and [Ru]@SILP-C-2. This demonstrates that [Ru]@SILP-B-2 has the maximum Ru per mass unit of SILP[Cl]-X, which is consistent with the ICP results (Table S2†). TEM images of [Ru]@SILP with the different ILs show that the Ru species has the most even size and is distributed uniformly in [Ru]@SILP-A-2 compared to the other two samples (Fig. 2c). Besides this, the lattice fringe of Ru in [Ru]@SILP-A-2 is clearly observed to have a spacing of 0.195 nm,[54] which further confirms the successful immobilization of Ru. In contrast to their round shape in [Ru]@SILP-A-2 and [Ru]@SILP-B-2, the Ru in the [Ru]@SILP-C-2 exhibits randomly ellipsoid shapes with a particle size of more than 20 nm, indicating that the Ru therein is agglomerated.

The FT-IR spectra of IL, SILP[Cl] and [Ru]@SILP were recorded to detect the potential variation of the functional groups therein. The set of IL-A, SILP[Cl]-A and [Ru]@SILP-A-2 was selected as representatives for discussion and their spectra are displayed in Fig. 3. Meanwhile, the spectrum of silica gel was also studied for comparison. The broad band at 1236–1043 cm^{-1} can be assigned to the asymmetric stretching

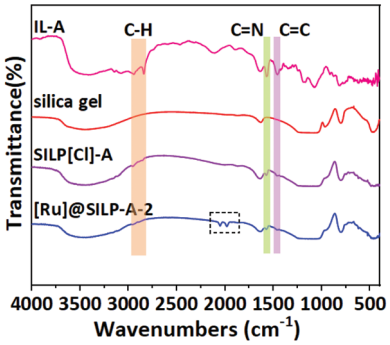

Fig. 3 FT-IR spectra of IL-A, silica gel, SILP[Cl]-A and [Ru]@SILP-A-2.

vibration of Si–O–Si, and the peaks at 804 and 470 cm^{-1} belong to the symmetric stretching vibration and bending vibration of Si–O, respectively. Besides these, a broad, asymmetric feature is detected at 3457 cm^{-1}, which can be attributed to O–H vibrations of either the silanol or water in silica gel. The main absorption peaks of IL-A can be observed at 1575 and 1461 cm^{-1}, assigned to the C=N and C=C stretching vibrations of the imidazole ring, respectively. Additionally, typical aliphatic C–H stretching can be observed at 2948 and 2842 cm^{-1}. As expected, the FT-IR spectrum of SILP[Cl]-A shows both characteristic peaks of silica gel and IL-A, suggesting the successful incorporation of IL-A into the silica gel. In comparison, two new absorption peaks at 2051 and 1980 cm^{-1} are present in the spectrum of [Ru]@SILP-A-2, which can be assigned to Ru-hydride-carbonyl-carbene species according to the literature.[44] The other spectra of IL-X, SILP[Cl]-X and @SILP-X-2 (X = B and C) are displayed and compared in Fig. S2.† Both display identical variations in the functional groups compared to when X = A.

The surface modification was further studied from the ^{29}Si and ^{13}C cross-polarization magic angle spinning nuclear magnetic resonance (CP-MAS NMR) spectra of [Ru]@SILP-A-2, SILP[Cl]-A and silica gel (Fig. 4). The spectrum of silica gel displays three ^{29}Si resonances at −111 (Q^4), −102 (Q^3) and −91 (Q^2) ppm, which can be assigned to $Si(OSi)_4$, $Si(OSi)_3OH$ and $Si(OSi)_2(OH)_2$ species, respectively (Fig. 4A-a). Upon sequential functionalization with IL-A and incorporation of Ru species,

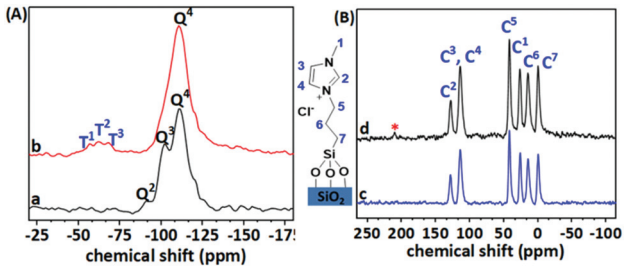

Fig. 4 Solid-state NMR studies. (A) Solid-state ^{29}Si CP-MAS NMR spectra of (a) silica gel and (b) [Ru]@SILP-A-2; (B) solid-state ^{13}C CP-MAS NMR spectra of (c) SILP[Cl]-A and (d) [Ru]@SILP-A-2.

both the Q^3 and Q^2 peaks disappear, while the Q^4 peak is retained (Fig. 4A-b), indicating the condensation of singular and geminal silanol groups with the trimethoxysilane moiety. Besides this, the spectrum of [Ru]@SILP-A-2 displays three additional signals at −52 (T^1), −61 (T^2), and −67 (T^3) ppm, assigned to R-Si(OSi)(OMe)$_2$, R-Si(OSi)$_2$(OMe), and R-Si(OSi)$_3$, respectively. These results unambiguously confirm the covalent attachment of IL-A on the surface and in the channels of the silica gel support. Noteworthily, no resonance was detected at the lower field over −50 ppm, suggesting the absence of physically adsorbed silane molecules. Meanwhile, the ^{13}C CP-MAS NMR spectrum of SILP[Cl]-A further confirmed the successful modification of silica gel with IL-A (Fig. 4B-c). Evidently, typical imidazolium ^{13}C peaks at 114.1 (C^3, C^4) and 128.3 (C^2) ppm were detected. Besides these, the signals at 26.0 (C^1), 0.34 (C^7), 14.51 (C^6) and 41.8 (C^5) ppm can be attributed to the methyl (C^1) and three methylene (C^5, C^6, C^7) groups in IL-A, respectively. Upon incorporation of $Ru_3(CO)_{12}$, a new peak at 210.3 ppm appears in the ^{13}C spectrum of [Ru]@SILP-A-2 (Fig. 4B-d), which can be assigned to the ligated carbonyl group at the Ru site.

X-ray photoelectron spectroscopy (XPS) was employed to further characterize the chemical composition and state of the newly prepared hybrids (Fig. 5). The XPS survey profile of [Ru]@SILP-A-2 features a combination of characteristic peaks of SILP[Cl]-A and Ru (Fig. 5a). Noteworthily, the quite weak peak of Ru 3p in the profile is due to a low concentration of Ru. The two resolved peaks of N 1s at around 399.7 and 401.8 eV can be respectively assigned to the amine nitrogen atom and ammonium nitrogen atom within the imidazolium ring (Fig. 5b). Besides these, the peaks at 197.4 eV (Cl $2p_{3/2}$) and 198.8 eV (Cl $2p_{1/2}$) in the high-resolution spectrum suggest the presence of chloride anions (Fig. 5c). These values were found to be almost the same as that for [Ru]@SILP-C-2, but relatively lower than those of [Ru]@SILP-B-2 (197.6 and 199.1 eV) (Fig. S4†). This suggests that there are more chloride anions at or near the surface of [Ru]@SILP-A-2 and [Ru]@SILP-C-2 compared to [Ru]@SILP-B-2. In addition, the binding energy of Ru $3p_{3/2}$ and $3p_{1/2}$ can be observed at 462.4 and 484.5 eV, respectively, confirming the presence of Ru (0) in [Ru]@SILP-A-2 (Fig. 5d).[55] Remarkably, both peaks show an upshift of *ca.* 0.5 eV compared to those of $Ru_3(CO)_{12}$, suggesting the formation of a Ru active site with a strong interaction between the imidazolium unit and Ru(0).

The amount of ILs decorated in the [Ru]@SILP-X-2 was quantified by elemental analysis (Table S3†). Taking nitrogen as the indicator atom, the IL concentration in [Ru]@SILP-X-2 was recorded as 29.4 wt% (X = A), 24.3 wt% (X = B), and 41.7 wt% (X = C), respectively. Thus, the corresponding molar percentages of IL-X decorated on the surface and in the channels of the silica gel are 88.2% (X = A), 56.0% (X = B), and 98.1% (X = C) under identical conditions. The apparently low value for [Ru]@SILP-B-2 can be probably attributed to the hydrophobic characteristics of IL-B, thereby leading to significant resistance upon diffusion onto the surface and into the channels of the hydrophilic silica gel. All these results are consistent with the BET characterization. [Ru]@SILP-B-2 exhibits a higher surface area compared to [Ru]@SILP-A-2, which can be attributed to the lower percentage of IL decoration in the former. However, the flexible hydrocarbon C_{12} chains on the imidazole ring of IL-B can seriously block the channels, leading to a poorer pore volume. Similarly, [Ru]@SILP-C-2 exhibits the lowest surface area and porosity when the percentage of decorated IL is almost the same as that of [Ru]@SILP-A-2.

The thermal stability of the newly prepared [Ru]@SILP-X-2 and the silica gel support was investigated by carrying out thermogravimetric analysis (TGA) under a nitrogen atmosphere (Fig. 6). The first weight loss of all of the samples occurred at about 50 °C, which can be attributed to the physically adsorbed water and residual organic solvents present from the preparation of the hybrids being lost. The second weight loss of [Ru]@SILP-X-2 in the range of between 230 and 350 °C can likely be attributed to the partial decomposition of the ILs, such as the end group alkyl chains decorated on the imidazolium ring. Singh[56] supposed that this follows a phe-

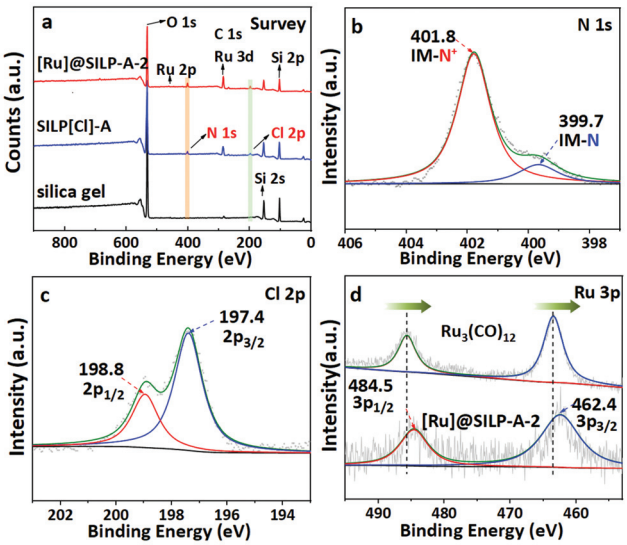

Fig. 5 XPS studies. (a) XPS survey spectra of silica gel, SILP[Cl]-A and [Ru]@SILP-A-2; (b) N 1s; (c) Cl 2p and (d) Ru 3p in [Ru]@SILP-A-2.

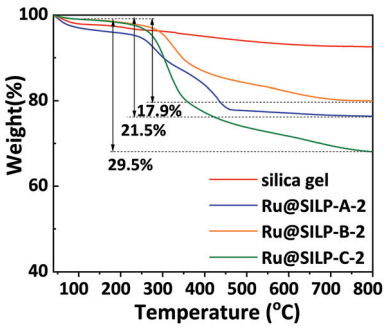

Fig. 6 TGA curves of silica gel and [Ru]@SILP-X-2 (X = A, B and C).

nomenological 'hinged spring' model, wherein the surface oxygen atom of the silica gel interacts with the C–H groups of the imidazolium ring to 'hinge' it better to the pore walls while the end alkyl chains will be exposed outside the pore. Thus, the alkyl chains are more easily broken under thermolysis than the imidazolium ring. Noteworthily, the decomposition of ILs is accompanied by that of $Ru_3(CO)_{12}$, according to the literature.[57] The last weight reduction in the range of between 350 °C and 800 °C is likely due to the full decomposition of the ILs. As a result, the weight loss of [Ru]@SILP-X-2 was calculated to be up to 21.5% (X = A), 17.9% (X = B), and 29.5% (X = C), values that are less than the mass of the respective IL and $Ru_3(CO)_{12}$ loaded. We therefore suppose that the ILs and $Ru_3(CO)_{12}$ are partially confined in the inner pores of the silica gel, which has good pyrolysis resistance. Collectively, these results demonstrate that the immobilized ILs are thermally stable at temperatures of lower than 230 °C, ensuring the reliability of catalytic performance screening on [Ru]@SILP within this limit.

The CO_2 adsorption capability of the silica gel and [Ru]@SILP-X-2 were investigated and the CO_2 adsorption isotherms were measured at pressures of up to 1.0 bar at 273 and 298 K, respectively (Fig. 7). Clearly, the silica gel exhibits a relatively higher adsorption capacity, which can be attributed to the strong affinity between the CO_2 and the hydroxyl groups decorated in the channel of the porous silica gel and higher pore volume therein. Upon the introduction of ILs, the CO_2 uptake of [Ru]@SILP-X-2 decreased compared to that of the silica gel support (Fig. 7a). Besides this, [Ru]@SILP-A-2 has a better storage capacity than [Ru]@SILP-B-2 and [Ru]@SILP-C-2 under identical conditions. As expected, the CO_2 uptake capacity of all of the samples decreased when the temperature increased from 273 to 298 K. The isosteric heat of adsorption (Q_{st}) value of CO_2 for [Ru]@SILP-X-2 was subsequently calculated using the virial method. Evidently, [Ru]@SILP-A-2 has the highest value of 21.3–29.0 kJ mol^{-1} compared to the other two hybrids (Fig. 7b).

Catalytic performance evaluation for the alkoxycarbonylation of olefins with CO_2

The catalytic performance of the [Ru]@SILP-X hybrids was subsequently evaluated towards the alkoxycarbonylation of olefins with CO_2 as a C1 surrogate, together with some controlled experiments for comparison. Taking the methoxycarbonylation of cyclohexene (**1a**) with CO_2 as the benchmark reaction (Fig. 8a), [Ru]@SILP-A-2 displays outstanding catalytic performance under 4 MPa CO_2 at 160 °C for 20 h, leading to the formation of ester (**2a**) in 74% yield with a TON value of 81 (Fig. 8b). In comparison, neither [Ru]@SILP-B-2 nor [Ru]@SILP-C-2 provide a comparable yield under identical conditions. We supposed that the higher loading amount of Ru but lower percentage of decorated IL in [Ru]@SILP-B-2 meant that it does not have sufficient reactive sites for the reaction. Besides this, the flexible hydrocarbon C_{12} chains of IL-B not only block the pores but also inhibit the access of reactants to the catalytic active sites. The latter is also responsible for the poor performance of [Ru]@SILP-C-2. We also found that a appropriate loaded amount of Ru with SILP[Cl]-A as the support was crucial to the reactivity (Fig. 8c). As a result, either insufficient or excess loading of Ru is not conducive to the number of active sites per unit mass of substrate. Varying of the reaction conditions, such as the solvents, temperatures, chloride additives and pressure of CO_2, was examined (Fig. 8d and Fig. S5†). We supposed that a similar Ru species was formed to that in either the water–gas shift reaction[58] or the reverse water–gas shift reaction[42] catalyzed by [Ru]@SILP, wherein the presence of both Cl^- and CO is highly likely. Under optimized conditions, a higher catalytic activity than the homogeneous systems can be achieved by [Ru]@SILP-A-2, leading to an 87% yield of **2a** with a TON value of 94. In addition, CO and H_2 can be detected in the gas mixture, leading to TONs of 3.6 and 1.8, respectively (Fig. S6†).

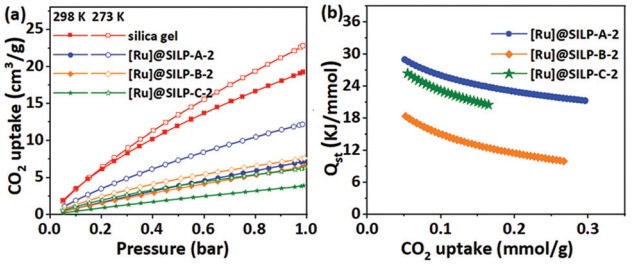

Fig. 7 CO_2 adsorption capability evaluation. (a) CO_2 adsorption isotherms of silica gel and [Ru]@SILP-X-2 recorded at 273 and 298 K; (b) the respective isosteric heats of adsorption for CO_2 of [Ru]@SILP-X-2.

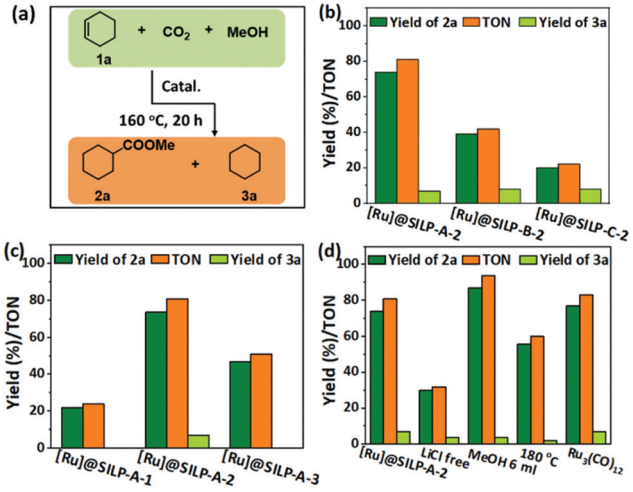

Fig. 8 Catalytic performance evaluation. (a) Scheme of the benchmark reaction. Reaction conditions: **1a** (2 mmol), catalyst (2.8 mol% Ru), LiCl (4 mmol, 2 equiv.), MeOH (4 ml), CO_2 (4 MPa), 160 °C, 20 h; yield was determined by GC-FID analysis using isooctane as an internal standard; (b) reactivity comparison among [Ru]@SILP-X-2; (c) reactivity comparison among [Ru]@SILP-A-*m*; *m* = 1 (0.028 mmol Ru g^{-1}), *m* = 2 (0.056 mmol Ru g^{-1}), *m* = 3 (0.104 mmol Ru g^{-1}); (d) other cross experiments.

With the optimal [Ru]@SILP-A-2 catalyst in hand, the olefin tolerance of this newly developed protocol was next examined (Fig. 9). All reactions were conducted in the presence of [Ru]@SILP-A-2 (2.8 mol% Ru) at 160 °C under 4 MPa CO_2 for 20 h. We found that the small cyclic olefin performed better than the large one (**1b** *vs.* **1c**), which might be attributed to the difference in the steric hindrance in the pores of [Ru]@SILP-A-2. Besides this, the yield of ester from the long-chain terminal olefin (**1e**) was worse than that from the short-chain olefin (**1d**) due to high diffusion resistance in the pore channels. To our surprise, a branched ester is slightly preferred over a linear one in both cases. It is worth noting that the opposite selectivity in the carbonylation of olefins with CO_2 has been well documented using both $Ru_3(CO)_{12}$[14] and Rh-PR_3[59] homogeneous catalysts. We suppose that this is probably due to the steric confinement effect of the support and the acidity of the silica gel.[60] Besides this, significant isomerization was detected in the reaction of 2-octene (**1e′**), leading to an identical result to that of 1-octene (**1e**). It is rationally supposed that the isomerization of 2-octene is much faster than methoxycarbonylation with CO_2 using this protocol. Finally, diene substrates, such as isoprene (**1f**) and 1,3-cyclohexadiene (**1g**), were also examined, which provided the corresponding mono carboxylic ester rather than double methoxycarbonylation product with the second olefin site being reduced.

The recyclability of [Ru]@SILP-A-2 (Fig. 10) and [Ru]@SILP-B-2 (Fig. S7†) were finally examined by repeated addition of **1a** after each run. After four runs, the yields of ester product **2a** were 82% and 35%, respectively, suggesting only a slight reduction in the catalytic activity of [Ru]@SILP-A-2 and [Ru]@SILP-B-2. To address this issue, full characterization of the used [Ru]@SILP-A-2 was conducted. FT-IR study demonstrated that the characteristic peaks of the silica gel, IL-A and Ru complexes were retained in their spectra, compared to the fresh hybrids (Fig. S8†). Besides this,

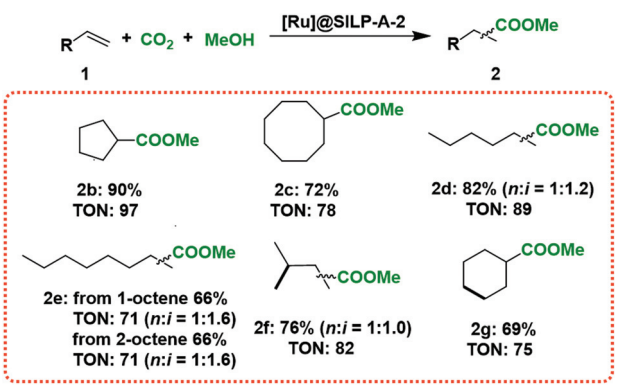

Fig. 9 Screening the olefin scope of the [Ru]@SILP-A-2-catalyzed alkoxycarbonylation with CO_2. Reaction conditions: **1** (2 mmol), [Ru]@SILP-A-2 (2.8 mol% Ru), LiCl (4 mmol, 2 equiv.), MeOH (6 ml), CO_2 (4 MPa), 160 °C, 20 h; the yield was determined by GC analysis using the area normalization method. Only linear products are shown, and the bold bonds represents the hydrogenation of the double bond.

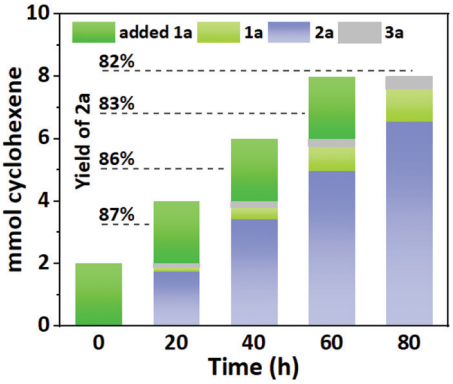

Fig. 10 Examination of the recyclability of [Ru]@SILP-A-2. Reaction conditions: **1a** (2 mmol), [Ru]@SILP-A-2 (2.8 mol% Ru), MeOH (6 ml), CO_2 (4 MPa), 160 °C, 20 h; yield was determined by GC-FID analysis using isooctane as an internal standard.

the SEM images showed no obvious changes in the used [Ru]@SILP-A-2, suggesting that the silica skeleton is less affected during the recycling (Fig. S9†). However, the elemental analysis results show that the nitrogen content decreased by 0.55%, suggesting the leaching of IL-A from the catalyst (Table S3†).

Conclusions

In summary, the first example of heterogeneous catalysis in the alkoxycarbonylation of olefins with CO_2 is reported. The [Ru]@SILP catalyst was synthesized by immobilization of a ruthenium complex on SILP, wherein imidazolium chloride was used to decorate the surface or channels of the silica gel support. Different IL films, by varying the functionality at the imidazolium cation, strongly affect the porosity, active Ru sites, and CO_2 adsorption capacity of [Ru]@SILP, thereby considerably affecting the activity of the resulting catalysts. The optimized [Ru]@SILP-A-2 catalysts displays enhanced catalytic performance compared to an independent homogeneous system for the alkoxycarbonylation of olefins with CO_2 under identical conditions, attributed to the highly dispersed catalytic sites, porous framework with high surface area, and large CO_2 absorption capacity and enrichment. Besides this, it shows prominent substrate selectivity, wherein small cyclic olefins and short-chain linear olefins were preferred, corresponding to the steric hindrance effect of the pore channels. The fabrication of heterogeneous IL-based catalysts suitable for the coupling of CO_2 with olefins based on this newly developed novel design concept is now under way in our lab.

Experimental section

Synthesis of SILP[Cl]-X

The synthesis of 1-R-3-(trimethoxysilyl)propyl imidazolium chloride (IL-X; R = Me (X = A), $C_{12}H_{25}$ (X = B), $(CH_2CH_2O)_3CH_3$ (X = C)) is described in detail in the ESI.† SILP[Cl]-X was sub-

sequently synthesized by chemical functionalization of silica gel with IL-X according to previous reports, wherein X denotes the type of IL incorporated. In a typical procedure, silica gel (5 g) and IL-X (8.9 mmol) were dispersed in toluene (50 mL) in a 100 ml Schlenk bottle. The mixture was refluxed at 110 °C for 24 h under a nitrogen atmosphere. After filtration and washing with MeOH (6 × 10 ml), the solid was subjected to Soxhlet extraction with MeOH (100 ml) for 24 h to remove excess ILs. The obtained SILP[Cl]-X was dried at 90 °C for 12 h under high vacuum and then stored in a glove box.

Synthesis of [Ru]@SILP-X-*m*

[Ru]@SILP-X-*m* was synthesized by reacting SILP[Cl]-X (2 g) with a certain amount of $Ru_3(CO)_{12}$, based on the IL loading (m = 1, $Ru_3(CO)_{12}$ = 19 mg; m = 2, $Ru_3(CO)_{12}$ = 38 mg; m = 3, $Ru_3(CO)_{12}$ = 76 mg). Taking [Ru]@SILP-X-2 as an example, degassed THF (8 mL) was introduced into a mixture of SILP[Cl]-X (2 g) and $Ru_3(CO)_{12}$ (38 mg, 0.06 mmol) in a 50 mL Schlenk flask under a nitrogen atmosphere. After stirring at 120 °C for 16 h, the solid was isolated by filtration and washed thoroughly with THF (3 × 10 ml) and MeOH (3 × 10 ml) to remove unreacted $Ru_3(CO)_{12}$. The residue was then dried under vacuum at 80 °C for 12 h to give [Ru]@SILP-X-2.

General procedure for the catalytic performance examination of [Ru]@SILP

A typical experiment was carried out under argon using a standard glovebox, and [Ru]@SILP-X-2 (2.8 mol% Ru), LiCl (170 mg, 4 mmol), MeOH (4 ml) and olefins (2 mmol) were added to a 30 mL autoclave equipped with a Teflon lining. Then, CO_2 (40 bar) was introduced, and the autoclave was heated to 160 °C. After reaction for 20 h, the mixture was cooled down and the pressure was released. The reaction solution was diluted with MeOH, followed by filtration using an organic filter. The filtrate was then analyzed by GC using isooctane as an internal standard. GC analysis was performed using an Agilent GC-7890B spectrometer equipped with a capillary column (DB-FFAP, 30 m × 0.32 mm) using a flame ionization detector. The temperatures of the injector and FID were both controlled at 250 °C. The components were separated according to the following program: an initial temperature of 100 °C held for 2 min, heated to 200 °C at a rate of 25 °C min^{-1} and then held for 5 min. The calculation equations for ester yield and turnover number (TON) are as follows:

$$Y_{ester}\% = (\text{moles of the produced ester} / \text{moles of initial olefins}) \times 100\%$$

$$TON_{ester} = \text{moles of the produced ester} / \text{moles of } Ru_3(CO)_{12} \text{ in the catalyst}$$

Recyclability examination of [Ru]@SILP

The recyclability of [Ru]@SILP was examined according to the literature.[61] Specifically, after the first run, the mixture was cooled down and the pressure released. The autoclave was then opened inside the glovebox and a mixture of fresh **1a** (2 mmol), MeOH (1 ml) and isooctane (1 ml) was added for the next run. Before the start of each run, one drop was taken out from the mixture with a syringe to detect the distribution of the composition by GC analysis. After the appointed runs, the used catalyst was separated from the mixture upon filtration, which was then washed with MeOH (6 × 20 ml) and dried under high vacuum at 80 °C for 24 h.

Conflicts of interest

There are no conflicts to declare.

Acknowledgements

Financial support from the Excellent Young Scientists Fund (22022815), the Key Research Program of Frontier Sciences, CAS (ZDBS-LY-JSC022), the National Natural Science Foundation of China (U1704251, 22078336, 21374029), and Zhengzhou High Level Talent Certificate (20180200052) is gratefully acknowledged.

References

1 R.-P. Ye, J. Ding, W. Gong, M. D. Argyle, Q. Zhong, Y. Wang, C. K. Russell, Z. Xu, A. G. Russell, Q. Li, M. Fan and Y.-G. Yao, *Nat. Commun.*, 2019, **10**, 5698–5712.
2 W. Zhou, J. Guo, S. Shen, J. Pan, J. Tang, L. Chen, C. Au and S. Yin, *Acta Phys.–Chim. Sin.*, 2020, **36**, 1906048–1906058.
3 A. Weilhard, M. I. Qadir, V. Sans and J. Dupont, *ACS Catal.*, 2018, **8**, 1628–1634.
4 M. I. Qadir, F. Bernardi, J. D. Scholten, D. L. Baptista and J. Dupont, *Appl. Catal., B*, 2019, **252**, 10–17.
5 J. Klankermayer, S. Wesselbaum, K. Beydoun and W. Leitner, *Angew. Chem., Int. Ed.*, 2016, **55**, 7296–7343.
6 J. Artz, T. E. Mueller, K. Thenert, J. Kleinekorte, R. Meys, A. Sternberg, A. Bardow and W. Leitner, *Chem. Rev.*, 2018, **118**, 434–504.
7 Q. Liu, L. Wu, R. Jackstell and M. Beller, *ChemCatChem*, 2014, **6**, 2805–2809.
8 P. H. Gehrtz, V. Hirschbeck and I. Fleischer, *Chem. Commun.*, 2015, **51**, 12574–12577.
9 S. C. Stouten, T. Noel, Q. Wang, M. Beller and V. Hessel, *Catal. Sci. Technol.*, 2016, **6**, 4712–4717.
10 X. Zhang, C. Shen, C. Xia, X. Tian and L. He, *Green Chem.*, 2018, **20**, 5533–5539.
11 T. Fujihara, T. H. Xu, K. Semba, J. Terao and Y. Tsuji, *Angew. Chem., Int. Ed.*, 2011, **50**, 523–527.
12 S. H. Li, W. M. Yuan and S. M. Ma, *Angew. Chem., Int. Ed.*, 2011, **50**, 2578–2582.
13 C. M. Williams, J. B. Johnson and T. Rovis, *J. Am. Chem. Soc.*, 2008, **130**, 14936–14937.

14 L. Wu, Q. Liu, I. Fleischer, R. Jackstell and M. Beller, *Nat. Commun.*, 2014, **5**, 3091–3096.
15 J. Cored, A. Garcia-Ortiz, S. Iborra, M. J. Climent, L. Liu, C. H. Chuang, T. S. Chan, C. Escudero, P. Concepcion and A. Corma, *J. Am. Chem. Soc.*, 2019, **141**, 19304–19311.
16 J. Liu, C. Li, F. Wang, S. He, H. Chen, Y. Zhao, M. Wei, D. G. Evans and X. Duan, *Catal. Sci. Technol.*, 2013, **3**, 2627–2633.
17 L. Roldan, Y. Marco and E. Garcia-Bordeje, *ChemSusChem*, 2017, **10**, 1139–1144.
18 J. Polanski, T. Siudyga, P. Bartczak, M. Kapkowski, W. Ambrozkiewicz, A. Nobis, R. Sitko, J. Klimontko, J. Szade and J. Lelatko, *Appl. Catal., B*, 2017, **206**, 16–23.
19 Y. Zhou, N. Han and Y. Li, *Acta Phys.–Chim. Sin.*, 2020, **36**, 2001041–2001051.
20 C. P. Mehnert, *Chem. – Eur. J.*, 2005, **11**, 50–56.
21 A. Riisager, R. Fehrmann, M. Haumann and P. Wasserscheid, *Top. Catal.*, 2006, **40**, 91–102.
22 B. Xin and J. Hao, *Chem. Soc. Rev.*, 2014, **43**, 7171–7187.
23 J. Bruenig, Z. Csendes, S. Weber, N. Gorgas, R. W. Bittner, A. Limbeck, K. Bica, H. Hoffmann and K. Kirchner, *ACS Catal.*, 2018, **8**, 1048–1051.
24 R. Castro-Amoedo, Z. Csendes, J. Bruenig, M. Sauer, A. Foelske-Schmitz, N. Yigit, G. Rupprechter, T. Gupta, A. M. Martins, K. Bica, H. Hoffmann and K. Kirchner, *Catal. Sci. Technol.*, 2018, **8**, 4812–4820.
25 L.-L. Lou, X. Peng, K. Yu and S. Liu, *Catal. Commun.*, 2008, **9**, 1891–1893.
26 Y. Yang, C. Deng and Y. Yuan, *J. Catal.*, 2005, **232**, 108–116.
27 X. Guo, Z. Peng, A. Traitangwong, G. Wang, H. Xu, V. Meeyoo, C. Li and S. Zhang, *Green Chem.*, 2018, **20**, 4932–4945.
28 K. L. Luska, A. Bordet, S. Tricard, I. Sinev, W. Gruenert, B. Chaudret and W. Leitner, *ACS Catal.*, 2016, **6**, 3719–3726.
29 K. L. Luska, P. Migowski, S. El Sayed and W. Leitner, *ACS Sustainable Chem. Eng.*, 2016, **4**, 6186–6192.
30 L. Offner-Marko, A. Bordet, G. Moos, S. Tricard, S. Rengshausen, B. Chaudret, K. L. Luska and W. Leitner, *Angew. Chem., Int. Ed.*, 2018, **57**, 12721–12726.
31 M. Haumann, M. Jakuttis, R. Franke, A. Schoenweiz and P. Wasserscheid, *ChemCatChem*, 2011, **3**, 1822–1827.
32 M. Jakuttis, A. Schoenweiz, S. Werner, R. Franke, K.-D. Wiese, M. Haumann and P. Wasserscheid, *Angew. Chem., Int. Ed.*, 2011, **50**, 4492–4495.
33 S. Shylesh, D. Hanna, S. Werner and A. T. Bell, *ACS Catal.*, 2012, **2**, 487–493.
34 S. Walter, H. Spohr, R. Franke, W. Hieringer, P. Wasserscheid and M. Haumann, *ACS Catal.*, 2017, **7**, 1035–1044.
35 S. El Sayed, A. Bordet, C. Weidenthaler, W. Hetaba, K. L. Luska and W. Leitner, *ACS Catal.*, 2020, **10**, 2124–2130.
36 D. Geier, P. Schrnitz, J. Walkowiak, W. Leitner and G. Francio, *ACS Catal.*, 2018, **8**, 3297–3303.
37 G. Moos, M. Emondts, A. Bordet and W. Leitner, *Angew. Chem.*, 2020, **59**, 11977–11983.
38 M. J. Schneider, M. Haumann and P. Wasserscheid, *J. Mol. Catal. A: Chem.*, 2013, **376**, 103–110.
39 D. Blaumeiser, R. Stepic, P. Wolf, C. R. Wick, M. Haumann, P. Wasserscheid, D. M. Smith, A.-S. Smith, T. Bauer and J. Libuda, *Catal. Sci. Technol.*, 2020, **10**, 252–262.
40 S. Werner, N. Szesni, A. Bittermann, M. J. Schneider, P. Haerter, M. Haumann and P. Wasserscheid, *Appl. Catal., A*, 2010, **377**, 70–75.
41 P. Wolf, M. Aubermann, M. Wolf, T. Bauer, D. Blaumeiser, R. Stepic, C. R. Wick, D. M. Smith, A.-S. Smith, P. Wasserscheid, J. Libuda and M. Haumann, *Green Chem.*, 2019, **21**, 5008–5018.
42 T. Yasuda, E. Uchiage, T. Fujitani, K.-i. Tominaga and M. Nishida, *Appl. Catal., B*, 2018, **232**, 299–305.
43 M. J. Schneider, M. Lijewski, R. Woelfel, M. Haumann and P. Wasserscheid, *Angew. Chem., Int. Ed.*, 2013, **52**, 6996–6999.
44 M. Ali, A. Gual, G. Ebeling and J. Dupont, *ChemCatChem*, 2014, **6**, 2224–2228.
45 M. Ali, A. Gual, G. Ebeling and J. Dupont, *ChemSusChem*, 2016, **9**, 2129–2134.
46 M. I. Bruce, M. L. Cole, R. S. Fung, C. M. Forsyth, M. Hilder, P. C. Junk and K. Konstas, *Dalton Trans.*, 2008, **31**, 4118–4128.
47 H. Lebel, M. K. Janes, A. B. Charette and S. P. Nolan, *J. Am. Chem. Soc.*, 2004, **126**, 5046–5047.
48 J. A. Cabeza, I. del Rio, D. Miguel and M. G. Sanchez-Vega, *Chem. Commun.*, 2005, 3956–3958.
49 S. Jaaskelainen and M. Haukka, *Appl. Catal., A*, 2003, **247**, 95–100.
50 G. Lavigne, *Eur. J. Inorg. Chem.*, 1999, 917–930.
51 V. K. Srivastava and P. Eilbracht, *Catal. Commun.*, 2009, **10**, 1791–1795.
52 K. Tominaga and Y. Sasaki, *J. Mol. Catal. A: Chem.*, 2004, **220**, 159–165.
53 L. Wu, Q. Liu, R. Jackstell and M. Beller, *Org. Chem. Front.*, 2015, **2**, 771–774.
54 Y. Yao, D. S. He, Y. Lin, X. Feng, X. Wang, P. Yin, X. Hong, G. Zhou, Y. Wu and Y. Li, *Angew. Chem., Int. Ed.*, 2016, **55**, 5501–5505.
55 B. M. Faroldi, J. F. Múnera and L. M. Cornaglia, *Appl. Catal., B*, 2014, **150–151**, 126–137.
56 M. P. Singh, R. K. Singh and S. Chandra, *J. Phys. D: Appl. Phys.*, 2010, **43**, 092001–092004.
57 T. Huang, B. Liu, Z. Zhang, Y. Zhang and J. Li, *RSC Adv.*, 2014, **4**, 28529–28536.
58 S. Werner, N. Szesni, R. W. Fischer, M. Haumann and P. Wasserscheid, *Phys. Chem. Chem. Phys.*, 2009, **11**, 10817–10819.
59 T. G. Ostapowicz, M. Schmitz, M. Krystof, J. Klankermayer and W. Leitner, *Angew. Chem., Int. Ed.*, 2013, **52**, 12119–12123.
60 Z. He, Z. Hou, Y. Luo, Y. Dilixiati and W. Eli, *Catal. Sci. Technol.*, 2014, **4**, 1092–1103.
61 J. Brünig, Z. Csendes, S. Weber, N. Gorgas, R. W. Bittner, A. Limbeck, K. Bica, H. Hoffmann and K. Kirchner, *ACS Catal.*, 2018, **8**, 1048–1051.

